

Neural evidence for attentional capture by salient distractors

Received: 6 July 2023

Accepted: 21 February 2024

Published online: 27 March 2024

 Check for updates

Rongqi Lin^{1,2,3,4,5,6,10}, Xianghong Meng^{7,10}, Fuyong Chen^{8,10}, Xinyu Li⁵, Ole Jensen⁹, Jan Theeuwes⁶ & Benchi Wang^{1,2,3,4}✉

Salient objects often capture our attention, serving as distractors and hindering our current goals. It remains unclear when and how salient distractors interact with our goals, and our knowledge on the neural mechanisms responsible for attentional capture is limited to a few brain regions recorded from non-human primates. Here we conducted a multivariate analysis on human intracranial signals covering most brain regions and successfully dissociated distractor-specific representations from target-arousal signals in the high-frequency (60–100 Hz) activity. We found that salient distractors were processed rapidly around 220 ms, while target-tuning attention was attenuated simultaneously, supporting initial capture by distractors. Notably, neuronal activity specific to the distractor representation was strongest in the superior and middle temporal gyrus, amygdala and anterior cingulate cortex, while there were smaller contributions from the parietal and frontal cortices. These results provide neural evidence for attentional capture by salient distractors engaging a much larger network than previously appreciated.

Rapidly orienting towards salient objects in a crowded environment has played a crucial role in human evolution, as it permits us to quickly identify potential prey, mates or predators. This inherent human trait also makes us vulnerable, as our attention can be captured by salient objects around us. For instance, we are often distracted by our phone's buzzer when focusing on a task. Similarly, during visual search tasks in a laboratory setting, certain types of stimuli that stand out from the environment (for example, a red circle surrounded by green stimuli), known as salient objects, automatically capture our attention^{1,2} regardless of their relevance to our immediate goals^{3–6}; this gives rise to the phenomenon of attentional capture. Research over the past few decades has revealed behavioural evidence on how salient objects (distractors) capture our attention and the properties of salient distractor processing³ (for review, see refs. 1,7). Despite this, there has been a fierce debate

regarding whether or not salient objects capture attention automatically. Although this debate has not yet been resolved by behavioural studies, the present study on intracranial electroencephalography (iEEG) recordings might help by providing direct evidence regarding the neural dynamics and brain regions in the human brain responsible for attentional capture and the ways in which salient distractors interact with our current goals.

Circumstantial evidence supporting salient distractor processing in the brain is mainly provided by neurophysiological studies conducted in non-human primates. These studies have shown that neuronal activity increases in the visual, parietal and frontal cortices when salience signals are present in the receptive field^{8–13}. This activity decreases after monkeys have been trained to ignore the salience signals that act as distractors^{14–16}. Although these experiments provide

¹Key Laboratory of Brain, Cognition and Education Sciences, South China Normal University, Ministry of Education, Guangzhou, China. ²Institute for Brain Research and Rehabilitation, South China Normal University, Guangzhou, China. ³Center for Studies of Psychological Application, South China Normal University, Guangzhou, China. ⁴Guangdong Key Laboratory of Mental Health and Cognitive Science, South China Normal University, Guangzhou, China. ⁵Department of Psychology, Zhejiang Normal University, Jinhua, China. ⁶Department of Experimental and Applied Psychology, Vrije Universiteit Amsterdam, Amsterdam, the Netherlands. ⁷Department of Neurosurgery, Shenzhen University General Hospital, Shenzhen, China. ⁸Department of Neurosurgery, University of Hongkong Shenzhen Hospital, Shenzhen, China. ⁹Centre for Human Brain Health, School of Psychology, University of Birmingham, Birmingham, UK. ¹⁰These authors contributed equally: Rongqi Lin, Xianghong Meng, Fuyong Chen. ✉e-mail: wangbenchi.swift@gmail.com

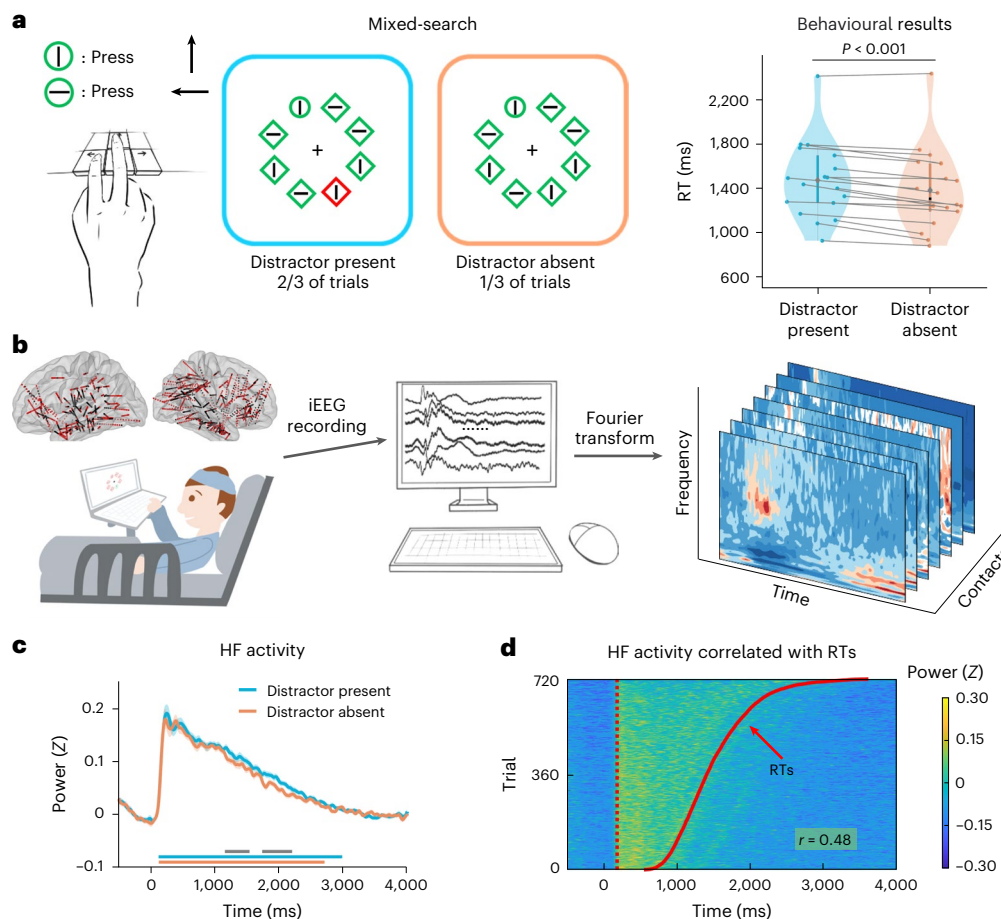


Fig. 1 | Stimuli, behavioural results and HF activity. **a**, Display set-up and possible locations of search elements. The participants searched for one unique shape (the target) among the search elements (for example, a circle among diamonds) and indicated whether the line segment inside the target was vertical or horizontal by pressing the ‘up’ or ‘left’ key as fast as possible. The rightmost panel shows the behavioural results (two-tailed test); the violin plots show the full distribution of $n = 18$ participants, and the dots correspond to individual RTs. **b**, Intracranial EEG data were recorded while the participants performed the visual search task, from which HF (60–100 Hz) power was extracted. The left

panel indicates possible locations of the contacts in various brain areas. Red dots indicate locations of responsive contacts. **c**, The observed HF power between the distractor-present and distractor-absent conditions, with data variance represented by ± 1 s.e.m. Significant areas are highlighted by solid lines, and the grey lines mark significant differences between conditions (cluster-based permutation test, $P < 0.01$). **d**, Trial-by-trial (Pearson) correlations between the time of peak HF activity and the RT. The dashed red line indicates the start of HF activity by visual inspection (180 ms), and the solid red line indicates the trial-specific RTs.

important insight into the neural mechanisms underlying salient distractor processing, they typically involve recording neuronal activity from small and often restricted retinotopic locations (that is, receptive fields)^{17,18}, making it difficult to track the targets (current goals) and distractors simultaneously and thus limiting our understanding of how they interact. Similarly, non-invasive electrophysiological studies in humans that measure event-related potential components (the N2pc and Pd) to characterize neural responses to salient distractors also evaluate target or distractor processing individually¹⁹. It is important to note that target and distractor processing in these studies^{17–19} are never assessed within the same group of trials; that is, they are never evaluated within the same time frame. These findings therefore need to be complemented by human intracranial studies uncovering the full network involved in the simultaneous processing of distractors and targets in relation to attentional capture.

Developing a comprehensive theory of attentional capture requires a deep understanding of how the human brain handles salient distractors. To explore this, we examined iEEG recordings from 18 neurosurgical patients performing a visual search task^{3,4}, which offered a unique opportunity to investigate the neuronal responses related to salient distractor processing in the human brain with optimal anatomical precision and high temporal resolution. Moreover,

a well-established inverted encoding model^{20–22} (IEM), which can track spatial attention in neuroscientific studies (for review, see ref. 23), was applied to track the spatial tunings originating from the target and the distractor simultaneously in high-frequency (HF) activity (60–100 Hz). This representational specific multivariate approach enabled us to dissociate the processing of salient distractors from that of targets and provided the time course for the target and distractor processing, to examine when and how distractors interacted with the current goals. Additionally, by tracking neural responses towards salient distractors across various brain regions, we identified whether distinct brain regions exhibited activity specific to the distractor representation and how they interacted with each other.

Results

In our visual search task, participants searched for a unique shape (the target) among search elements while keeping fixation at the centre and responded to the orientation of the line segment inside the target (Fig. 1a). The target was present on each trial, while in the distractor-present condition, a uniquely coloured distractor was randomly present in two thirds of the trials (see Methods for the details), and the participants were asked to ignore it. We also tested another session before the present experiment, in which only the target was

present throughout the whole session for practising; its results can be found in the Supplementary Information (Supplementary Fig. 1). As shown in Fig. 1a, a paired t -test showed that the mean response times (RTs) were slower when a salient distractor was present (1,480 ms) than when it was absent (1,390 ms) ($t_{17} = 6.37, P < 0.001$ (corrected for false discovery rate (FDR)), Cohen's $d = 1.5$). Consistent with other studies^{3,4} (for review, see refs. 1,7), the slower RTs in the distractor-present condition provide evidence for attentional capture.

HF activity

We first identified 1,275 responsive contacts (after removing 7.5% of responsive contacts that were identified as potentially correlated with epileptic seizure; see Methods for the details) that showed HF (60–100 Hz) activity during the experiment (see Supplementary Table 1 for individual numbers). The HF activity occurred in the 120–2,986 ms and 124–2,710 ms intervals for the distractor-present and distractor-absent conditions, respectively. Note that in the presence of a salient distractor, the initial burst of HF activity reduced slowly, resulting in higher power from 1,154 to 1,540 ms and from 1,736 to 2,204 ms relative to the distractor-absent condition (Fig. 1c), reflecting a prolonged visual search process due to the involvement of the salient distractor. This conclusion was based on the observation that HF activity is typically stronger during challenging searches that produce slower responses²⁴, as well as on the association of HF activity with neuronal processing including sustained attention (for review, see ref. 25). The results for other low-frequency bands can be found in Supplementary Fig. 2a,b.

We further examined the relationship between HF activity and participants' RTs. To do this, we initially sorted individual trial-specific RTs and then calculated their average across participants. Subsequently, we conducted a Pearson correlation analysis. The results revealed a significant trial-by-trial correlation between the time of peak HF activity and RT ($r = 0.48, P < 0.001$) (Fig. 1d). In sum, HF activity is correlated with behavioural responses, which might reflect the processing of targets and salient distractors. We examined this by further isolating the target and distractor neuronal responses using a multivariate analysis.

IEM reconstruction of HF activity

To track the processing of targets and salient distractors, we applied an IEM²² (see Fig. 2a and Methods for the details). Overall, spatial attention towards the target and salient distractor was reconstructed from HF activity, beginning approximately 200 ms after the onset of the search array, and persisted over time (see Supplementary Fig. 3 for reconstructed HF channel-tuning functions (CTFs) across time for each of eight locations). As shown in Fig. 2b, the positive target-tuning CTF slopes (reflecting the spatial tuning of population-level HF activity towards the target) were significant in the 230–338 ms and 348–590 ms intervals in the distractor-absent condition, while in the distractor-present condition, target-tuning CTF slopes were significantly above zero in the 308–538 ms and 560–772 ms intervals

(cluster-based permutation test, $P < 0.01$). Note that when a salient distractor was introduced in the distractor-present condition, target-tuning CTF slopes were notably reduced in the early time window (236–302 ms; cluster-based permutation test, $P < 0.01$), and the latency was significantly later ($t_{17} = 6.43, P < 0.001$, Cohen's $d = 1.52$) than in the distractor-absent condition. This implies that spatial attention was captured by the salient distractor, leading to less effective processing of the target.

The current results, depicted in Fig. 2c (left), indicate the simultaneous tracking of spatial attention towards the salient distractor and the target. The distractor-tuning CTF slopes (reflecting the spatial tuning of population-level HF activity towards the distractor) were significantly above zero in the 218–546 ms interval. It is worth noting that the magnitude of distractor-tuning CTF slopes was stronger than that of target-tuning CTF slopes in the early time window (228–302 ms; cluster-based permutation test, $P < 0.01$), and its latency was significantly earlier ($t_{17} = 4.32, P < 0.001$, Cohen's $d = 1.02$), indicating an initial and rapid processing of the salient distractor; this suggests a cortical mechanism that swiftly reacts to a pop-out signal¹⁴. Additionally, distractor-related attention declined quickly, as its CTF slopes were lower than the target ones in the late time window from 568 ms to 664 ms (cluster-based permutation test, $P < 0.01$). No activity was detected for the non-responsive contacts (Fig. 2c, right), and we were not able to reconstruct early spatial attention (before 400 ms) towards the target from other low-frequency bands (see Supplementary Fig. 2c,d for the details). In sum, this indicates that the initial processing of salient distractors is short-lived, but they still capture our attention.

Further analyses were conducted to investigate whether early processing of distractors and targets was related to participants' behavioural responses. We first divided all trials according to fast and slow responses for each participant (median split). Following this, we applied the IEM to the fast and slow trials per participant and observed that for fast trials, the target-tuning CTF slopes were significantly above zero in the 278–764 ms interval (cluster-based permutation test, $P < 0.01$), whereas no significant effects were observed for the distractor. For slow trials, the target-tuning CTF slopes were significantly above zero in the 318–404 ms interval, while the positive distractor-tuning CTF slopes emerged earlier in the 236–322 ms interval (Fig. 2d). This indicates that early distractor-related processing delays behavioural responses.

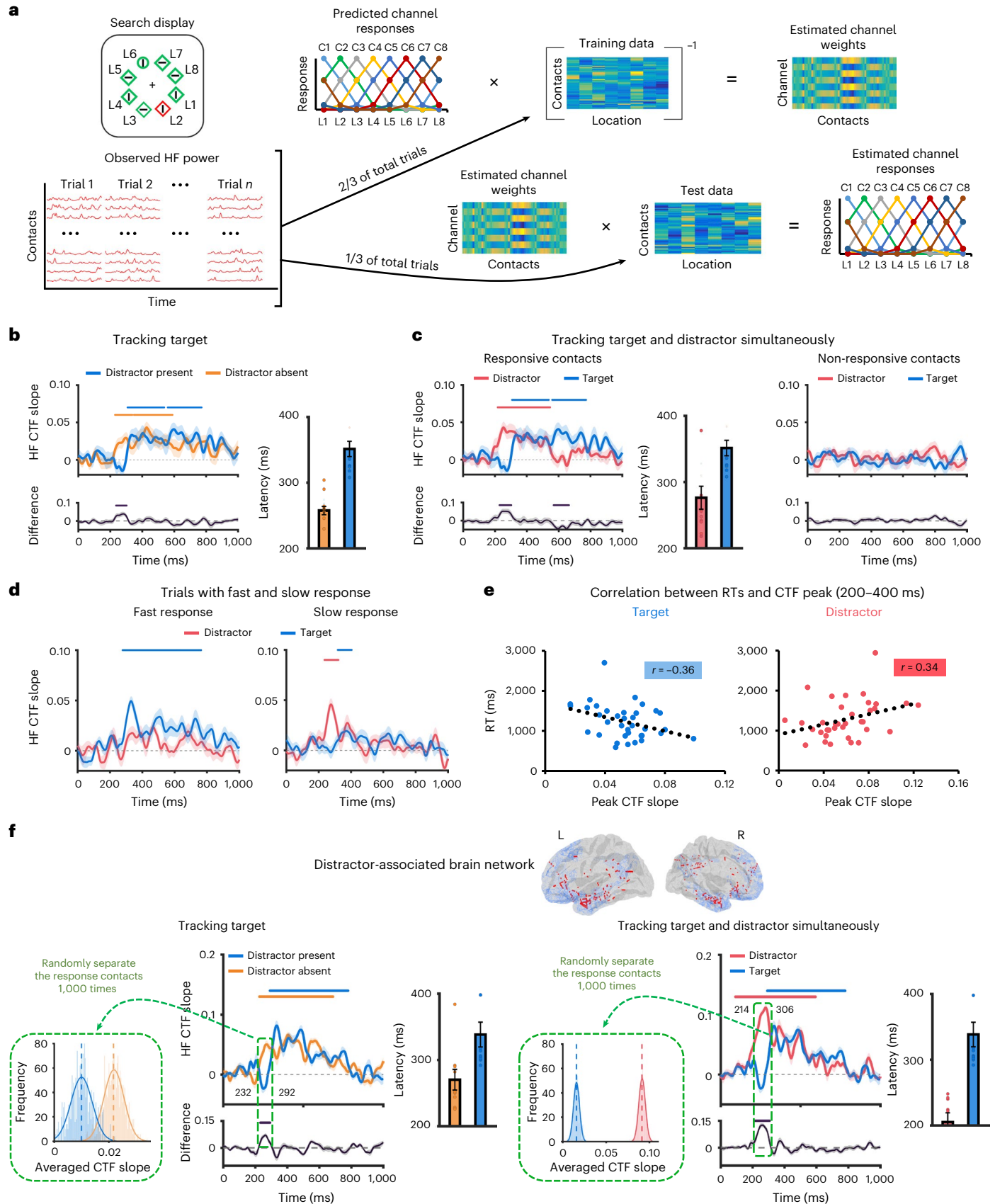
We also examined the correlation between the peak CTF slope and behavioural RT for targets and distractors separately. For fast and slow trials per participant, we calculated the mean RTs and selected the peak CTF slope within the early time window (200–400 ms). The results showed a negative correlation between mean RT and the peak target CTF slope ($r = -0.36, P = 0.03$) but a positive correlation between mean RT and the peak distractor CTF slope ($r = 0.34, P = 0.042$) (Fig. 2e). These findings further support the notion that early processing of distractors drives subsequent behavioural responses.

Fig. 2 | Signal reconstruction with the IEM. **a**, Illustration of the IEM. The search elements are situated at eight locations (L1 to L8) around a fixation cross, and each spatially selective channel (C1 to C8) is tuned for one of the eight possible locations. **b**, Spatial selectivity (measured as CTF slopes) for the target in both the distractor-present and distractor-absent conditions, including the absent-minus-present difference in the magnitude and latency of the CTF slopes ($n = 18$ participants, two-tailed). **c**, Spatial selectivity for the target and salient distractors in the distractor-present condition for responsive and non-responsive contacts. The distractor-minus-target difference in the magnitude and latency of the CTF slopes is also shown ($n = 18$ participants, two-tailed). **d**, Spatial selectivity for the target and salient distractors in the distractor-present condition for fast and slow trials. **e**, The correlation between the peak CTF slopes and behavioural RTs for the target and distractor. **f**, The results obtained using the random-group strategy for responsive contacts located in

the distractor-associated brain network ($n = 20$ groups, two-tailed tests). The left panel shows the spatial selectivity for the target in the distractor-present and distractor-absent conditions, including the absent-minus-present difference in the magnitude and latency of the CTF slopes, and the distribution of the target-tuning averaged CTF slopes from 1,000 IEM reconstructions. The right panel shows the spatial selectivity for the target and salient distractors in the distractor-present condition, including the distractor-minus-target difference in the magnitude and latency of the CTF slopes, and the distribution for the target- and distractor-tuning averaged CTF slopes from 1,000 IEM reconstructions. The green dashed outlines indicate the time windows used to estimate the averaged CTF slopes for calculating the distribution. The solid dots within each bar plot represent individual data points. The data variance is represented by ± 1 s.e.m. Significant CTF selectivity (or significant difference) areas are highlighted by solid lines (cluster-based permutation test, $P < 0.01$).

In the present study, salient distractors were never positioned at the same location as the target. That is, they occupied different locations in each distractor-present trial. Given that we were simultaneously tracking both the target and salient distractor, one might question

whether the CTF slopes for salient distractors exhibit a covariation with those for the target. In such a scenario, one would anticipate a correlation in the latency and peak of the CTF slopes between tracking the target and tracking the salient distractor. However, our findings do



not support this hypothesis, as no such correlation was observed (both $r < 0.29$, $P > 0.24$) (Supplementary Fig. 4a).

Moreover, by creating one classifier in a support vector machine according to HF power to classify eight target or salient distractor locations in the distractor-present condition, we were able to decode the processing of target and salient distractor locations. The support vector machine decoding results showed that the classification accuracy for the salient distractor exceeded chance level (1/8) in the 216–470 ms interval, while that for the target exceeded chance level during the intervals of 294–446 ms, 542–832 ms and 844–926 ms (Supplementary Fig. 4b; additional information regarding methods can be found in the Supplementary Information). This reanalysis based on support vector machines rather than IEMs confirms the early and rapid detection of salient distractors.

Identifying the distractor-associated brain network

Using the IEM, we were able to simultaneously track the processing of the target and salient distractor across all responsive contacts. However, it is possible that certain brain areas contribute more significantly to the processing of and interaction between the target and the salient distractor. To explore this possibility, we grouped responsive contacts into six smaller brain networks based on large-scale cerebral networks²⁶ to further localize certain brain areas specific to salient distractor processing. The sole purpose of using this brain network template was to group responsive contacts into functionally defined brain areas.

It should be noted that the number of responsive contacts in each brain network varied greatly across participants (Supplementary Table 2). This variability made it impractical to apply the IEM separately to each brain network for every participant. To mitigate this issue, we employed a random-group strategy, where we randomly grouped all responsive contacts across participants into groups of at least eight contacts each per brain network. We assumed that the responses in contacts from different participants within the same brain area should be similar. If spatial attention towards salient distractors is governed by a single brain area, it should be reconstructed in the IEM regardless of how the contacts within this brain area are distributed, whether within or across participants (Supplementary Fig. 5). We validated the random-group strategy by dividing all responsive contacts into 20 groups (mimicking a group of 20 participants) and replicating the critical results from the raw group of 18 participants with high statistical power (refer to Supplementary Fig. 5 and the corresponding text in the Supplementary Information for more detailed information).

To determine which brain areas are mainly involved in the processing of and interaction between the target and the salient distractor, we applied the random-group strategy (validated on all responsive contacts) separately for six different brain networks based on large-scale cerebral networks²⁶. We identified two brain networks (linked to the default and limbic systems) that were primarily engaged in handling both the target and the salient distractor (Supplementary Figs. 6 and 7; more detailed results regarding each brain network can be found in the Supplementary Information). Thus, in further analysis, we combined these areas and referred to them as the distractor-associated brain network. The results for this distractor-associated brain network replicated those found for all responsive contacts (Fig. 2f; the details can be found in the Supplementary Information). Critically, in the distractor-present condition, compared with the distractor-absent condition, target-tuning CTF slopes were significantly lower in the early time window (232–292 ms; cluster-based permutation test, $P < 0.01$). Additionally, in the distractor-present condition, the magnitude of distractor-tuning CTF slopes was stronger than that of target-tuning CTF slopes in the early time window (214–306 ms; cluster-based permutation test, $P < 0.01$). It would also be interesting to incorporate the target-associated brain network as a focal point in future studies.

Note that this critical result observed in the distractor-associated network was not attributed to arbitrary placement of contacts.

To address this concern, we iterated the grouping of contacts 1,000 times to generate distributions of the averaged CTF slopes (from 232 ms to 292 ms) for the target in the distractor-present and distractor-absent conditions, and those of the averaged CTF slopes (from 214 ms to 306 ms) for the distractor and target in the distractor-present condition (see Methods for further details). The results revealed that the target-related distribution in the distractor-present condition differed significantly from that in the distractor-absent condition ($\chi^2_{49} = 1582.8$, $P < 0.001$, $w = 0.89$; w is the effect size for the chi-squared test), with averaged CTF slopes smaller for target-tuning in the distractor-present condition (Fig. 2f, left); and the distractor-related distribution differed significantly from the target-related distribution ($\chi^2_{49} = 2,000$, $P < 0.001$, $w = 1$), with averaged CTF slopes smaller for target-tuning than distractor-tuning (Fig. 2f, right). This confirms that the results were not due to arbitrary placement of contacts.

An extended network supporting salient distractor processing

Although we successfully identified the distractor-associated brain network, within this brain network it was unclear which brain regions dominated salient distractor processing the most and how the salient distractor was exchanged between these regions. Note that the number of contacts for each brain region varied significantly, and some of these regions did not have a sufficient number of contacts to apply the IEM. Thus, to investigate this further, we used a leave-one-out procedure to determine the contribution to distractor-related CTF slopes from each brain region. This approach was adopted on the basis of a previous study that used a similar method to investigate the contributions to neural representations from different brain regions²⁷. We assumed that if a particular brain region made the greatest contribution to the CTF slopes, excluding that region would cause the slopes to decline most dramatically, and vice versa (Fig. 3a). This procedure was repeated for 14 brain regions (which included at least ten responsive contacts, defined by the automated anatomical labeling template) located in the distractor-associated brain area. We first calculated the distribution of the averaged CTF slopes (from 214 ms to 306 ms, a time window showing significant CTF decoding for distractors in the distractor-associated brain network) and then created the same distribution after excluding each region. As shown in Fig. 3b, chi-squared tests revealed significant differences between the distribution from the distractor-associated area and the distribution created ($P < 0.001$, FDR corrected) for the superior temporal gyrus (STG) ($\chi^2_{49} = 1,515.16$, $w = 0.87$), amygdala (AMY) ($\chi^2_{49} = 1,756.13$, $w = 0.94$), middle temporal gyrus (MTG) ($\chi^2_{49} = 636.74$, $w = 0.57$), anterior cingulate cortex (ACC) ($\chi^2_{49} = 559.12$, $w = 0.53$), precuneus ($\chi^2_{49} = 116.79$, $w = 0.24$), inferior parietal (IP) ($\chi^2_{49} = 116.44$, $w = 0.24$), hippocampus ($\chi^2_{49} = 85.74$, $w = 0.21$) and prefrontal cortex (PFC) ($\chi^2_{49} = 203.76$, $w = 0.32$). The contribution was strongest from the AMY and decreased gradually from the STG to the MTG to the ACC (Fig. 3b,c). They all played major roles in salient distractor processing, as their exclusion led to a decline in CTF slopes. In contrast, the precuneus, IP, hippocampus and PFC offered only minor contributions to this process, as their exclusion led to an increase in CTF slopes. We do not discuss the other six brain regions (medial orbitofrontal cortex, lateral orbitofrontal cortex, inferior temporal gyrus, posterior cingulate cortex, parahippocampus and entorhinal) as we did not find significant changes in salient distractor processing when they were removed, but this does not discount their potential involvement in salient distractor processing and warrants further investigation.

We further computed the Jensen–Shannon (JS) divergence (where a positive JS value indicates a major contribution to salient distractor processing; see Methods for the details) for these brain regions, measuring the distance between created distributions. We showed that the JS divergence decreased as the contribution from each region decreased (from AMY to PFC; Fig. 3c). In brief, our analysis indicates

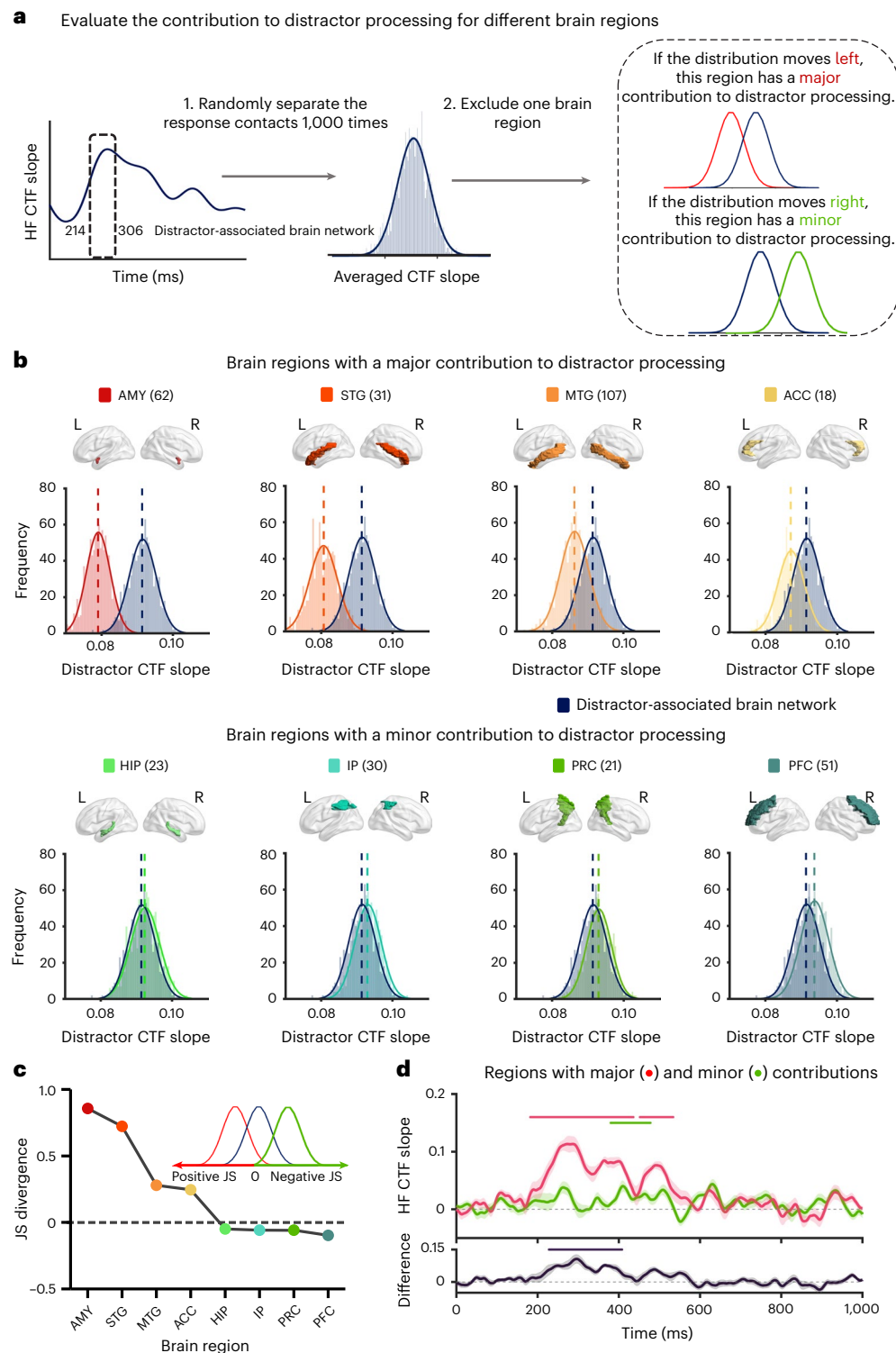


Fig. 3 | Contribution to salient distractor processing of different brain regions. **a**, Method for evaluating the contribution to salient distractor processing of different brain regions located in the distractor-associated brain network. The black dashed outline indicates the time window used to estimate the averaged distractor-related CTF slopes for calculating their distribution, which was obtained from 1,000 IEM reconstructions for 1,000 created random groups. By excluding one brain region to obtain the new distribution, we can determine whether this region has a relatively major or minor contribution to salient distractor processing. If the distribution moves left, this reflects a relatively major contribution; and if it moves right, this reflects a relatively minor contribution. The major and minor contributions were defined on the basis of their internal relationship. **b**, Brain regions (including the number of contacts) with significant

contributions (examined using the chi-squared test; see Methods for the details) to salient distractor processing and the created distributions after excluding each of them. HIP, hippocampus; PRC, precuneus. **c**, The JS divergence after excluding one major- or minor-contribution region. If the JS divergence is positive, this indicates that the distribution for the distractor-associated area is shifted to the left after excluding this brain region, reflecting a major contribution. Conversely, a negative value suggests a movement towards the right, reflecting a minor contribution. **d**, Spatial selectivity for salient distractors in the distractor-present condition for the major- and minor-contribution regions, including the major-minus-minor difference in the magnitude of CTF slopes. The data variance is represented by ± 1 s.e.m. Significant CTF selectivity (or significant difference) areas are highlighted by solid lines (cluster-based permutation test, $P < 0.01$).

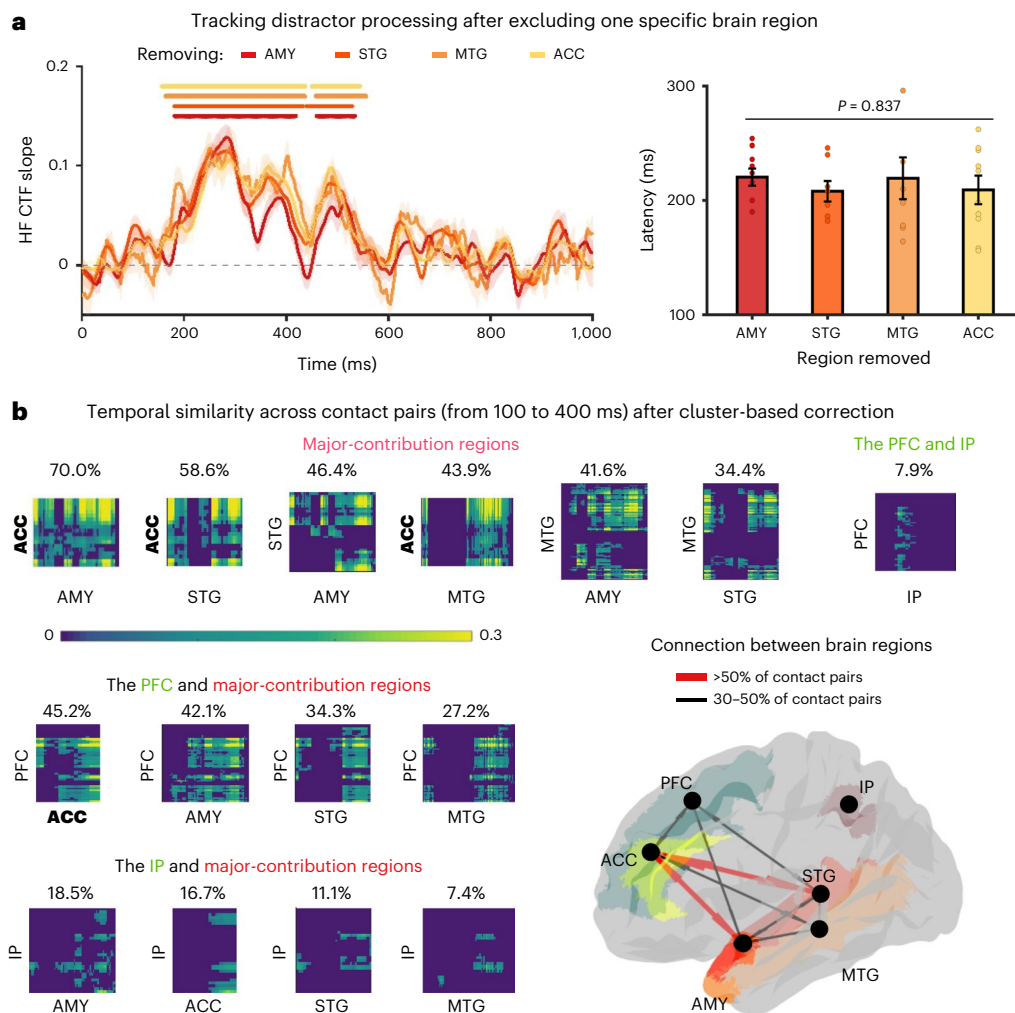


Fig. 4 | Comparisons between different brain regions when reacting to salient distractors. **a**, Spatial selectivity for the salient distractors in the distractor-present condition for the major-contribution regions after excluding each brain region, including the difference in the latency of the CTF slopes ($n = 10$ groups, two-tailed). The solid dots represent individual data points. The data variance is represented by ± 1 s.e.m. Significant CTF selectivity areas are highlighted by solid lines (cluster-based permutation test, $P < 0.01$). **b**, Temporal similarity (from 100 to 400 ms) across contact pairs between brain regions. The percentage

presented above each sub-figure indicates how many contact pairs between brain regions have significant connections (after cluster-based correction, $P < 0.01$). Bold labels indicate the brain region (ACC) that shows the strongest connections with other regions. The bottom right panel illustrates the connections between brain regions. The thick red lines indicate that the percentage of connections between regions is above 50%, and the thin black lines indicate that the percentage of connections between regions is between 30% and 50%.

that various brain regions contribute to salient distractor processing at different levels.

It is essential to appreciate that all these variations in CTF slopes, whether originating from major or minor regions, are linked to each other. We defined major regions as those for which excluding their contacts resulted in a smaller CTF slope in response to salient distractors. Conversely, the minor regions were defined as those for which excluding their contacts resulted in a larger CTF slope. In regard to the minor-contribution regions, three interpretations are possible. Distractor-related signals from these minor regions may exhibit positive, close-to-zero or negative CTF slopes. To further investigate which scenario is operative, we employed the IEM to track the attention towards salient distractors for both types of regions. The results revealed that distractor-related attention was successfully reconstructed from 182 ms to 436 ms and from 452 ms to 534 ms for the brain regions with major contributions, and from 380 ms to 478 ms for the brain regions with minor contributions (cluster-based permutation test, $P < 0.01$; Fig. 3d, top). Crucially, when directly compared with the minor-contribution regions, major-contribution regions generated bigger distractor-tuning CTF slopes (from 228 ms to

408 ms; cluster-based permutation test, $P < 0.01$; Fig. 3d, bottom). This confirms that salient distractors were represented more strongly and earlier in the major-contribution regions before engaging the minor-contribution regions.

We further used the leave-one-out procedure to examine whether any specific brain region within the major-contribution regions processed salient distractors first by excluding one brain region and conducting the IEM decoding again. As shown in Fig. 4a, the results showed that distractor-related attention was successfully reconstructed around similar time intervals—that is, 182–418 ms and 460–534 ms, 182–432 ms and 440–528 ms, 164–436 ms and 458–556 ms, and 156–436 ms and 450–544 ms for leaving out the AMY, STG, MTG and ACC, respectively. No significant difference was observed for their latencies ($F_{3,27} = 0.28$, $P = 0.837$, $\eta_p^2 = 0.03$), suggesting that salient distractors were processed in these brain regions simultaneously.

Functional connections when reacting to salient distractors

The AMY, STG, MTG and ACC might act as an integrated network to support salient distractor processing. We examined this by analysing the temporal correlation (from 100 to 400 ms) of HF power across contact

pairs between brain regions (that is, between-region similarity; see Methods for the details). Figure 4b illustrates significant similarities across contact pairs after cluster-based correction ($P < 0.01$). These results provide a tentative estimate for the dominating connectivity supporting salient distractor processing. In particular, the connection between the ACC and AMY (70% of contact pairs) was strongest, followed by the connection between the ACC and STG (58.6% of contact pairs) and then the AMY and STG (46.4% of contact pairs). This suggests that the ACC forms a hub to communicate with temporal lobe structures (see the illustration in Fig. 4b, right) in support of salient distractor processing. We also observed connections between the PFC and IP (7.9% of contact pairs), but this coupling was weaker than what we observed for the major-contribution regions (see the Supplementary Information for the connections between other minor-contribution regions). Further analysis revealed that the connections between the PFC and major-contribution regions were stronger (about 37.2% of contact pairs on average) than those between the IP and major-contribution regions (about 13.4% of contact pairs on average), suggesting that the PFC may play a role in linking major- and minor-contribution regions when reacting to salient distractors.

Discussion

The present study advances the understanding of attentional capture by salient distractors and its neural architecture in complex environments by analysing iEEG signals in humans. HF activity was linked to behavioural responses in a visual search task. From this HF activity, target- and distractor-tuning attention were successfully reconstructed and dissociated using a time-resolved multivariate approach (IEM decoding)^{20–22}. Importantly, when a salient distractor was introduced, attention was initially captured around 220 ms, with distractor-tuning attention boosted and target-tuning attention attenuated simultaneously. The contribution to this distractor-associated processing was dominated by the AMY, STG, MTG and ACC. The connectivity analysis suggests that the ACC might play an important role as a hub coordinating the processing of salient distractors in temporal lobe structures. This provides us with neural evidence for attentional capture by salient distractors engaging a much larger network than previously appreciated. In particular, the frontal and parietal cortex might play a secondary role compared with the ACC and temporal lobe structures.

In our study, we were unable to reconstruct spatial attention towards the target in the early time window (before 400 ms) from power in the alpha and beta bands (Supplementary Fig. 2b). Interestingly, we were able to reconstruct distractor-tuning attention from power in the HF band (60–100 Hz), a finding that has not previously been reported in human studies. Neurophysiology recordings in monkeys have demonstrated that the coherence in gamma activity between the parietal and frontal cortex mediates bottom-up attention in a single-feature search task²⁸, and inactivation of the parietal cortex reduces the power in (high-)gamma activity in the PFC and simultaneously causes the reduction of salience selection²⁹. Moreover, HF activity has previously been shown to be correlated with a wide range of cognitive functions, such as memory^{30,31}, attention³², learning³³ and language comprehension^{34,35}, underscoring its importance.

Gaining insight into the neural mechanisms for handling salient distractors is essential for any theory of attentional capture^{7,36–39}. Over the last 30 years, there has been a fierce debate over whether physically salient stimuli capture attention automatically or whether it is possible to prevent capture by salient stimuli^{1,7}. The idea of stimulus-driven attention posits that salient stimuli can automatically capture attention regardless of whether the salient stimulus is a target or a distractor^{1,3,40}. Our findings are consistent with such an interpretation, as the processing of salient distractors occurred early in time (around 220 ms) and simultaneously reduced target selection. It has recently been proposed that under specific conditions (which were not tested here), capture by salient stimuli may be prevented via

inhibitory top-down control processes^{41,42}. Further studies may be able to identify the neural suppression mechanisms that may prevent the occurrence of attentional capture by salient stimuli in advance to address the long-standing debate.

Previous studies involving scalp EEG revealed an event-related potential component (N2pc) when a salient distractor was presented laterally, signifying neural responses towards salient distractors^{19,43}. These findings provide insight into how the human brain processes salient distractors, but they do not necessarily reflect any simultaneous interaction between the processing of the target and salient distractors, as only one of them was investigated at a time. That is, these studies typically investigated distinct sets of trials to track these processes separately, but they never used the same set of trials to concurrently assess both target and distractor processing. As a result, these studies^{19,43} isolated target and distractor processing in different time frames. Notably, the event-related potential component N2pc (emerging around 250 ms) occurs later than the distractor-tuning attention (around 220 ms) reconstructed from HF activity in the present study. The attentional capture phenomenon identified in this study might therefore reflect a different mechanism than the N2pc. The comparison between scalp EEG and iEEG signals warrants further investigations.

Importantly, the STG, MTG, AMY and ACC (that is, the major-contribution regions) demonstrated activity specific to the distractor representation. The ACC, associated with novelty processing, has been observed to transiently activate in response to novel stimuli (that is, salient stimuli that stand out from the visual field) in both intracranial recordings⁴⁴ and functional MRI measurements^{45,46}. This is consistent with the ACC being one of the core regions in salience processing^{47,48}. Apart from this region, our findings from the STG and MTG relating to salient distractor processing are in line with previous research showing the involvement of the temporal cortex in early attentional selection, adjusting the attentional priority map^{49–51} (for review, see ref. 52). These studies have focused on goal-driven selection instead of salience-based selection, yet they implied that temporal areas could be involved in early salience processing, which we confirmed in the current study. In our study, the stronger connection between the ACC and temporal lobe structures might indicate that the ACC acts as a hub to coordinate the processing of salient distractors, warranting further investigations on the interaction between the key salient-distractor-associated regions.

Surprisingly, the AMY was also observed to be involved in salient distractor processing. Previous studies have indicated that the AMY plays an important role in biasing attention to alerting signals⁵³. This may indicate that the AMY determines the prioritization of salient distractors in general, as salient signals also alert us to potential threats in complex environments. Overall, we argue that the processing of salient distractors emerges from the interaction between these major-contribution regions, and these regions may act as an integrated network to support salient distractor processing.

Given the strong focus on the frontal and parietal cortex in previous studies conducted in non-human primates^{15,16}, it is surprising that these regions only contribute in a small and late albeit robust way to salient distractor processing. One possible reason is that neurons in the frontal and parietal regions merely respond selectively to the locations of salient stimuli and not to their features⁹. Similarly, the hippocampus might be linked to storing information about novel stimuli⁵⁴, such as the colour of the salient distractors, while the precuneus might be associated with spatial attention towards the locations of the salient distractors⁵⁵. Whatever the reason, our data suggest that these minor-contribution regions do not directly contribute to processing salient distractors, although they are part of the integrated network supporting the processing of salient distractors.

Temporoparietal junctions, as a core brain region in the ventral attention network that is typically recruited by unexpected events (for example, exogenous cues in the Posner task⁵⁶), are generally thought of as the brain region responsible for salience processing^{57,58}, driving our

initial exogenous attention. However, in the present study, we did not identify a brain region located at temporoparietal junctions, though we identified parietal and temporal brain regions responsible for salient distractor processing. To better understand the role of temporoparietal junctions in salient distractor processing, experiments should be done with sufficient electrode contact recordings in this region.

In sum, our findings suggest that the theories on the network contributing to salient distractor processing need to be revised to embrace the role of the ACC communicating with temporal lobe structures. This will be best done by multi-site recordings that allow us to investigate the network dynamics associated with salient distractor processing.

Methods

The present study was conducted according to the latest version of the Declaration of Helsinki and approved by the Medical Ethics Committee of Shenzhen University General Hospital (2018012).

Participants

Eighteen patients (9 males and 9 females, ages 21–58 years) at Shenzhen University General Hospital undergoing treatment for medication-resistant epilepsy participated in the present study. All patients had clinical depth electrodes implanted solely for diagnostic purposes as part of their evaluation for neurosurgical epilepsy treatment. Each depth electrode (0.8 mm in diameter) had 8, 10, 12, 14 or 16 contacts that were 1.5 mm apart and 2 mm in contact length. All participants gave verbal or written informed consent to participate in research, with no monetary compensation.

Paradigm and design

We adopted a visual search task^{3,39}, in which the participants had to maintain fixation throughout the trial. When the search array was briefly presented (4 s or until response), they were asked to search for one unique shape (the target) among the search elements (a circle among diamonds or a diamond among circles) and to indicate whether the line segment ($0.3^\circ \times 1.4^\circ$) inside the target was vertical or horizontal by pressing the 'up' or 'left' key as fast as possible (Fig. 1a). These unfilled shapes ($2^\circ \times 2^\circ$) with either a red or green outline were presented on an imaginary circle with a radius of 4° , centred at the fixation cross against a black background. If participants did not respond or pressed the wrong key, warning messages were given afterwards. Stimulus presentation and behavioural data collecting were controlled by custom scripts written in Python v.2.7 (ref. 59).

We introduced two conditions: the distractor-present and distractor-absent conditions. In both conditions, the target was present on each trial and was equally likely to be a circle or a diamond (Fig. 1). One third of the trials were distractor-absent trials; and two thirds of the trials were distractor-present trials, in which a uniquely coloured distractor (that is, a distractor singleton) was present, which had the same shape as the other neutral elements but a different colour (red or green with an equal probability). These two types of trials were mixed within each block (that is, a mixed-search design). The target and distractor (if present) appeared at each possible location with equal chance. After practising, the participants completed six blocks of 720 trials. There was a practice session in which only a target was present (Supplementary Fig. 1), three to six days before the actual start of the experiment; the results for this session can be found in the Supplementary Information.

Recordings and preprocessing

The iEEG data were acquired using a Nihon Kohden system at a sampling rate of 1,000 or 2,000 Hz. A common contact, used as the reference for the online recording data, was placed subcutaneously and recorded simultaneously with the depth electrodes. The offline preprocessing was performed in MATLAB v.2016 (MathWorks Inc.), using EEGLAB⁶⁰, ERPLAB⁶¹ and in-house MATLAB code. Contacts within each electrode

that were deemed noisy or corrupted upon visual inspection were excluded from further analysis. Signals were re-referenced to the average activity across all clean contacts and then resampled at 500 Hz. Common referencing is one of the most widely adopted referencing schemes for EEG recordings, as well as in iEEG studies^{62–64}. Some degree of dependency might be introduced between the contacts by the common reference scheme, but this would be minimal given the high number of contacts (approximately 143 contacts per participant). We removed 50 Hz power line noise prior to subsequent analyses using Hamming-windowed finite impulse response filters (order of 180) and then band-pass filtered the data from 0.3 to 200 Hz using a second-order Butterworth filter. For behaviour analysis, incorrect trials and trials on which the RTs were larger or smaller than 2.5 standard deviations from the average RT per participant were excluded.

Eye movements were not monitored in the present study given the complex clinical environment. While this may initially raise concerns, note that the present paradigm is intentionally designed to enable participants to perform the task without making eye movements. Importantly, previous studies employing the same paradigm and using an eye-tracker to control fixation (for example, see refs. 39,65) have shown results that are basically identical to the current findings. Moreover, other studies (for example, see refs. 66,67) employing a modified paradigm in which participants were forced to make eye movements towards the target showed that saccade latency towards the salient distractor was around 230 ms, which was slower than the onset of HF activity (around 120 ms; Fig. 1c) and the latency for distractor-related processing (around 220 ms; Fig. 2c,f) observed in our study. These findings indicate that eye movements are not likely to modulate HF activity, as the early, rapid detection of salient distractors reflected by the brain activity occur earlier than potential eye movements.

Electrode reconstruction and localization

We first registered post-operative computed tomography images to pre-operative T1-weighted MR images using FreeSurfer v.6.0.0 (ref. 68), following the iElvis pipeline⁶⁹. We inspected the quality of the registration and manually labelled each contact location on the T1-registered computed tomography images, which were then mapped onto a standard MNI space (Fig. 1b). To further determine the exact contact locations belonging to different brain areas and brain regions, we assigned contact MNI coordinates to each brain area according to large-scale cerebral networks (Yeo-7 template)²⁰ and to each brain region according to FreeSurfer's automatic parcellation. We went through each contact and assigned the closest cortical/subcortical label.

HF activity

HF activity (60–100 Hz) was considered to be the key electrophysiological marker of local neural population activity^{70–72} and to be correlated with attention⁷³, which is the focus of our interest. To extract HF activity, preprocessed iEEG data were broken into event-related epochs (–3 s to 6 s relative to the search onset, avoiding edge artefacts from wavelet convolution) and then were convolved with a set of Morlet wavelets with frequencies ranging from 1 to 150 Hz in 80 logarithmically spaced steps. The number of cycles of each wavelet was logarithmically spaced between 4 and 20 to strike a good balance between temporal and frequency precision. The HF power values within our focused epochs (–0.5 s to 4 s relative to the search onset) were Z-scored by subtracting the average value and dividing by the standard deviation across all trials.

To accurately compare HF power between conditions, we subtracted the mean HF power from –400 ms to –100 ms prior to the search onset for each condition separately and ran a cluster-based permutation test against a null distribution shuffled from 1,000 iterations (see 'Cluster-based permutation test' for the details) to make the comparison between conditions. We further correlated the time to reach the peak of HF activity with the RTs obtained from the search task via Pearson correlation.

Responsive contacts

Responsive contacts were identified by comparing the post-stimulus HF response (averaged over a time window from 100 ms to 400 ms) to the pre-stimulus baseline (averaged over a time window from -400 ms to -100 ms) using two-tailed, paired t -tests. The P values from all recording contacts (across all participants) were pooled together to control the FDR⁷⁴. Contacts that showed significant HF responses ($P_{\text{HF}} < 0.05$) were regarded as candidates for responsive contacts. We then compared the HF response for each time point after stimulus onset with the pre-stimulus baseline using paired t -tests ($P_{\text{HF}} < 0.05$). For each contact, if we could identify a time window of successive significant activities with a duration of over 200 ms, the contact was treated as responsive^{30,75}. This procedure was performed across participants, resulting in 1,379 contacts (see Supplementary Table 1 for the individual numbers). Note that no significant differences were observed in HF activity or the target- and distractor-related CTF slopes between all responsive contacts and the responsive contacts after excluding those that exhibited seizure-onset patterns as identified by neurosurgeons, and the responsive contacts showing seizure-onset patterns demonstrated similar HF activity as the unaffected ones (Supplementary Fig. 10). Nevertheless, we chose a more conservative approach by excluding the responsive contacts showing seizure-onset patterns (7.5% of all responsive contacts), resulting in 1,275 responsive contacts remaining for further analysis.

IEM

To reconstruct the attention towards the target and/or salient distractor, we applied an IEM²² to estimate spatial CTFs from the HF response across all responsive contacts over time (Fig. 2a). In accordance with previous studies^{21–23}, we specified an explicit model to represent how neural populations encode spatial information. This model focused exclusively on the spatial selectivity of the multivariate neural responses. To accomplish this, we constructed a basis set of eight spatial channels corresponding to the eight locations employed in the present study. The response profile of each spatial channel across element locations in the visual display was modelled as a half sinusoid raised to the seventh power:

$$R = \sin(0.5\theta)^7,$$

where θ is the element location (0–359°), and R is the response of the spatial channel in arbitrary units. Note that the response profile was circularly shifted to ensure that the peak response of each spatial channel centred over one of the eight element locations (22.5°, 67.5° and so on). The tuning curve for spatial channels was selected as a half-sine wave function because it maintains an approximately Gaussian shape (Fig. 2a), which mimics attentional response in a circular space. We opted for the seventh power, which aligns with previous studies^{21–23}.

We assumed that the HF power at each contact reflected the weighted sum of eight spatially selective channels (that is, neuronal populations), each tuned to a different angular location (corresponding to the possible locations of the search elements). We then partitioned our data randomly into independent sets of training data (2/3 of trials) and test data (1/3 of trials) following a cross-validation routine. The training data (B ; m contacts \times n locations) were used to estimate weights that approximated the possible contributions of the eight spatial channels to the observed HF responses measured at each contact and location. We defined C (k channels \times n locations) as a matrix of the predicted response of each spatial channel (estimated by the basic function for that channel) for each location, and W (m contacts \times k channels) as a weight matrix characterizing a linear mapping from channel space to contact space. We further described the relationships between B , C and W in a linear model as follows:

$$B = WC$$

Using the weight matrix (W) obtained via least-squares estimation, we inverted the model to transform the observed test data into estimated channel responses (that is, reconstructed CTFs). This IEM routine was iterated ten times to minimize the influence of idiosyncrasies specific to any trial assignment and obtain averaged channel-response profiles. We then calculated the slope of the CTFs via linear regression to quantify selective attentional processing for different locations over time. Higher slope values indicate greater attentional selectivity, while lower values indicate less attention selectivity. We reconstructed target-tuning and distractor-tuning CTFs according to the target location and salient distractor location, respectively, across participants. Note that the IEM assumed that each contact contained a large number of spatially selective neurons mainly tuned to a specific spatial location. The spatial tuning of a given contact was thus reflected by the combined response from the neurons detected by the contact. We analysed this by binning according to eight locations and calculated the corresponding weights for each contact. The calculated CTF slopes through these weights therefore represented the spatial tuning at the population level, originating from a group of spatially selective neurons.

To examine the CTF onset latency, we used a jackknife-based routine⁷⁶. CTF onset latency was measured as the earliest time at which the CTF slope reached 50% of its maximum amplitude within the first significant cluster for CTF selectivity. The latency difference (D) between conditions was measured as the difference in the latency of CTF slopes averaged across all participants. To estimate the standard error of the latency difference, $s.e._D$, we created subsamples that included all participants except one, and calculated the latency difference, D_{-i} (for $i = 1, \dots, N$, where N is the sample size), for each subsample. The jackknife estimate of the standard error ($s.e._D$) was calculated as

$$s.e._D = \sqrt{\frac{N-1}{N} \sum_{i=1}^N (D_{-i} - \bar{D})^2},$$

where \bar{D} is the mean of the latency differences obtained for all subsamples (that is, $\bar{D} = \sum D_{-i}/N$).

A jackknifed t statistic, t_j , was then calculated as

$$t_j = \frac{D}{s.e._D},$$

which follows an approximate t distribution with $N - 1$ degrees of freedom under the null hypothesis. Our jackknife test for latency differences was two-tailed.

Cluster-based permutation test

To correct for multiple comparisons, we used a cluster-based permutation test against a null distribution shuffled from 1,000 iterations (following the Monte Carlo randomization procedure). Specifically, a one-sample t -test was performed against zeros to identify above-chance CTF selectivity, and time windows with t values larger than a threshold ($P = 0.05$) were combined into contiguous clusters on the basis of adjacency. The cluster statistics was defined as the sum of the t values within each cluster. Moreover, the IEM procedure was repeated 1,000 times, but the location label was randomized within each group of trials so that the labels were independent of the observed responses in each contact. We identified the largest clusters for random location labels per iteration as described above, forming a null distribution of clusters. Clusters were determined to be significant if the cluster statistic was larger than the 99th percentile of the null distribution.

To make a between-conditions comparison on CTF selectivity or HF activity, paired t -tests were performed between the distractor-present and distractor-absent conditions. We followed the above routine to determine cluster statistics, but only the null distribution was formed by randomly permuting condition labels 1,000 times to get the largest clusters per iteration. Again, clusters

were determined to be significant if the cluster statistic was larger than the 99th percentile of the null distribution.

The distribution of the averaged CTF slopes and chi-squared test

The critical comparison in the present study was made between the distractor-tuning and target-tuning CTF slopes in the distractor-present condition. To avoid any potential doubt that our results from random groupings were selected arbitrarily, we determined the first significant cluster when comparing the distractor-tuning CTF slopes with target-tuning CTF slopes as the critical time window (Fig. 3), and we then averaged the CTF slopes for distractor- and target-tuning separately in this time window. Later, we iterated the grouping of contacts for the distractor- and target-related IEM reconstruction 1,000 times, obtaining distributions of the averaged CTF slopes for the distractor and target. To examine whether the distractor-related distribution was different from the target-related distribution, we applied the chi-squared test after creating 50 groups of CTF slopes for each distribution and applied FDR correction if necessary.

The JS divergence

The JS divergence is a measure of the distance between two probability distributions. It can be thought of as a measure of the degree of similarity between the two distributions. The JS divergence is a symmetrized version of the Kullback–Leibler (KL) divergence, which allows it to be used to compare any two probability distributions, regardless of which distribution is considered the reference and which is considered the comparison.

The JS divergence (JSD) between two probability distributions, P and Q , is defined as:

$$\text{JSD}(P|Q) = (\text{KL}(P|M) + \text{KL}(Q|M))/2,$$

where M is the ‘average’ distribution, defined as:

$$M = (P + Q)/2,$$

and $\text{KL}(P|Q)$ is the KL divergence between P and Q , defined as:

$$\text{KL}(P|Q) = \sum p(i) \times \log(p(i)/q(i)),$$

where the sum is taken over all possible values of i , and $p(i)$ and $q(i)$ are the probabilities of i in the distributions P and Q , respectively. If the distribution moved left, we gave the JS value a positive sign.

Temporal similarity analysis

The similarity across contact pairs was estimated using HF power in the distractor-present condition. To increase the signal-to-noise ratio²⁷, we obtained an averaged HF power from five randomly selected trials and iterated this routine 30 times. For each iteration, we correlated the time series of the averaged HF power within a 100–400-ms time window for each contact pair between different brain regions⁷⁷, obtaining Spearman’s r values. Note that the distractor processing was found to be significant in the distractor-associated brain network in the 214–306-ms interval, so a larger time window was chosen to include this critical period. The temporal similarity was calculated by averaging the temporal correlations (Spearman’s r values) across 30 iterations for each distractor location, which was then averaged across all locations. We Fisher Z -transformed all the correlation values for further analyses and applied the same cluster-based permutation test as mentioned above for CTF selectivity.

Reporting summary

Further information on research design is available in the Nature Portfolio Reporting Summary linked to this article.

Data availability

As the iEEG data are being used in ongoing studies, we are unable to share them at this time. However, should researchers express interest in replicating our study, we will share the derived iEEG data upon request.

Code availability

The code we used can be accessed through https://github.com/wangbenchi/Shared_data (ref. 78).

References

- Theeuwes, J. Top-down and bottom-up control of visual selection. *Acta Psychol.* **135**, 77–99 (2010).
- Itti, L. & Koch, C. Computational modelling of visual attention. *Nat. Rev. Neurosci.* **2**, 194–203 (2001).
- Theeuwes, J. Perceptual selectivity for color and form. *Percept. Psychophys.* **51**, 599–606 (1992).
- Theeuwes, J. Exogenous and endogenous control of attention: the effect of visual onsets and offsets. *Percept. Psychophys.* **49**, 83–90 (1991).
- Anderson, B. A., Laurent, P. A. & Yantis, S. Value-driven attentional capture. *Proc. Natl Acad. Sci. USA* **108**, 10367–10371 (2011).
- Schmidt, L. J., Belopolsky, A. V. & Theeuwes, J. Attentional capture by signals of threat. *Cogn. Emot.* **29**, 687–694 (2015).
- Luck, S. J., Gaspelin, N., Folk, C. L., Remington, R. W. & Theeuwes, J. Progress toward resolving the attentional capture debate. *Vis. Cogn.* **29**, 1–21 (2021).
- Constantinidis, C. & Steinmetz, M. A. Neuronal responses in Area 7a to multiple-stimulus displays: I. Neurons encode the location of the salient stimulus. *Cereb. Cortex* **11**, 581–591 (2001).
- Constantinidis, C. Posterior parietal cortex automatically encodes the location of salient stimuli. *J. Neurosci.* **25**, 233–238 (2005).
- Katsuki, F. & Constantinidis, C. Early involvement of prefrontal cortex in visual bottom-up attention. *Nat. Neurosci.* **15**, 1160–1166 (2012).
- Bichot, N. P., Schall, J. D. & Thompson, K. G. Visual feature selectivity in frontal eye fields induced by experience in mature macaques. *Nature* **381**, 697–699 (1996).
- Schall, J. D. & Hanes, D. P. Neural basis of saccade target selection in frontal eye field during visual search. *Nature* **366**, 467–469 (1993).
- Bichot, N. P. & Schall, J. D. Priming in macaque frontal cortex during popout visual search: feature-based facilitation and location-based inhibition of return. *J. Neurosci.* **22**, 4675–4685 (2002).
- Klink, P. C., Teeuwen, R. R. M., Lorteije, J. A. M. & Roelfsema, P. R. Inversion of pop-out for a distracting feature dimension in monkey visual cortex. *Proc. Natl Acad. Sci. USA* **120**, e2210839120 (2023).
- Ipata, A. E., Gee, A. L., Gottlieb, J., Bisley, J. W. & Goldberg, M. E. LIP responses to a popout stimulus are reduced if it is overtly ignored. *Nat. Neurosci.* **9**, 1071–1076 (2006).
- Cosman, J. D., Lowe, K. A., Zinke, W., Woodman, G. F. & Schall, J. D. Prefrontal control of visual distraction. *Curr. Biol.* **28**, 414–420 (2018).
- Moran, J. & Desimone, R. Selective attention gates visual processing in the extrastriate cortex. *Science* **229**, 782–784 (1985).
- Treue, S. & Trujillo, J. C. M. Feature-based attention influences motion processing gain in macaque visual cortex. *Nature* **399**, 575–579 (1999).
- Hickey, C., McDonald, J. J. & Theeuwes, J. Electrophysiological evidence of the capture of visual attention. *J. Cogn. Neurosci.* **18**, 604–613 (2006).
- Brouwer, G. J. & Heeger, D. J. Decoding and reconstructing color from responses in human visual cortex. *J. Neurosci.* **29**, 13992–14003 (2009).

21. Sprague, T. C. & Serences, J. T. Attention modulates spatial priority maps in the human occipital, parietal and frontal cortices. *Nat. Neurosci.* **16**, 1879–1887 (2013).
22. Foster, J. J., Sutterer, D. W., Serences, J. T., Vogel, E. K. & Awh, E. Alpha-band oscillations enable spatially and temporally resolved tracking of covert spatial attention. *Psychol. Sci.* **28**, 929–941 (2017).
23. Sprague, T. C., Saproo, S. & Serences, J. T. Visual attention mitigates information loss in small- and large-scale neural codes. *Trends Cogn. Sci.* **19**, 215–226 (2015).
24. Ossandon, T. et al. Efficient ‘pop-out’ visual search elicits sustained broadband gamma activity in the dorsal attention network. *J. Neurosci.* **32**, 3414–3421 (2012).
25. Clayton, M. S., Yeung, N. & Cohen Kadosh, R. The roles of cortical oscillations in sustained attention. *Trends Cogn. Sci.* **19**, 188–195 (2015).
26. Yeo, B. T. et al. The organization of the human cerebral cortex estimated by intrinsic functional connectivity. *J. Neurophysiol.* **106**, 1125–1165 (2011).
27. Kunz, L. et al. Hippocampal theta phases organize the reactivation of large-scale electrophysiological representations during goal-directed navigation. *Sci. Adv.* **5**, eaav8192 (2019).
28. Buschman, T. J. & Miller, E. K. Top-down versus bottom-up control of attention in the prefrontal and posterior parietal cortices. *Science* **315**, 1860–1862 (2007).
29. Chen, X. et al. Parietal cortex regulates visual salience and salience-driven behavior. *Neuron* **106**, 177–187 (2020).
30. Norman, Y. et al. Hippocampal sharp-wave ripples linked to visual episodic recollection in humans. *Science* **365**, eaax1030 (2019).
31. Solomon, E. A. et al. Widespread theta synchrony and high-frequency desynchronization underlies enhanced cognition. *Nat. Commun.* **8**, 1704 (2017).
32. Banaie Boroujeni, K., Oemisch, M., Hassani, S. A. & Womelsdorf, T. Fast spiking interneuron activity in primate striatum tracks learning of attention cues. *Proc. Natl Acad. Sci. USA* **117**, 18049–18058 (2020).
33. Gueguen, M. C. et al. Anatomical dissociation of intracerebral signals for reward and punishment prediction errors in humans. *Nat. Commun.* **12**, 3344 (2021).
34. Goldstein, A. et al. Shared computational principles for language processing in humans and deep language models. *Nat. Neurosci.* **25**, 369–380 (2022).
35. Khalighinejad, B., Herrero, J. L., Mehta, A. D. & Mesgarani, N. Adaptation of the human auditory cortex to changing background noise. *Nat. Commun.* **10**, 2509 (2019).
36. Gaspelin, N. & Luck, S. J. Inhibition as a potential resolution to the attentional capture debate. *Curr. Opin. Psychol.* **29**, 12–18 (2019).
37. Geng, J. J. Attentional mechanisms of distractor suppression. *Curr. Dir. Psychol. Sci.* **23**, 147–153 (2014).
38. Theeuwes, J., Bogaerts, L. & van Moorselaar, D. What to expect where and when: how statistical learning drives visual selection. *Trends Cogn. Sci.* **26**, 860–872 (2022).
39. Wang, B. & Theeuwes, J. Statistical regularities modulate attentional capture. *J. Exp. Psychol. Hum. Percept. Perform.* **44**, 13–17 (2018).
40. Jonides, J. & Yantis, S. Uniqueness of abrupt visual onset in capturing attention. *Percept. Psychophys.* **43**, 346–354 (1988).
41. Folk, C. L., Remington, R. W. & Johnston, J. C. Involuntary covert orienting is contingent on attentional control settings. *J. Exp. Psychol. Hum. Percept. Perform.* **18**, 1030–1044 (1992).
42. Gaspelin, N., Leonard, C. J. & Luck, S. J. Direct evidence for active suppression of salient-but-irrelevant sensory inputs. *Psychol. Sci.* **26**, 1740–1750 (2015).
43. Wang, B., Van Driel, J., Ort, E. & Theeuwes, J. Anticipatory distractor suppression elicited by statistical regularities in visual search. *J. Cogn. Neurosci.* **31**, 1535–1548 (2019).
44. Baudena, P., Halgren, E., Heit, G. & Clarke, J. M. Intracerebral potentials to rare target and distractor auditory and visual stimuli. III. Frontal cortex. *Electroencephalogr. Clin. Neurophysiol.* **94**, 251–264 (1995).
45. Clark, V. P., Fannon, S., Lai, S., Benson, R. & Bauer, L. Responses to rare visual target and distractor stimuli using event-related fMRI. *J. Neurophysiol.* **83**, 3133–3139 (2000).
46. Kiehl, K. A., Laurens, K. R., Duty, T. L., Forster, B. B. & Liddle, P. F. Neural sources involved in auditory target detection and novelty processing: an event-related fMRI study. *Psychophysiology* **38**, 133–142 (2001).
47. Uddin, L. Q. Saliency processing and insular cortical function and dysfunction. *Nat. Rev. Neurosci.* **16**, 55–61 (2015).
48. Menon, V. & Uddin, L. Q. Saliency, switching, attention and control: a network model of insula function. *Brain Struct. Funct.* **214**, 655–667 (2010).
49. Sani, I. et al. The human endogenous attentional control network includes a ventro-temporal cortical node. *Nat. Commun.* **12**, 360 (2021).
50. Stemann, H. & Freiwald, W. A. Evidence for an attentional priority map in inferotemporal cortex. *Proc. Natl Acad. Sci. USA* **116**, 23797–23805 (2019).
51. Bogadhi, A. R., Bollimunta, A., Leopold, D. A. & Krauzlis, R. J. Spatial attention deficits are causally linked to an area in macaque temporal cortex. *Curr. Biol.* **29**, 726–736 (2019).
52. Ramezani, H. & Fallah, M. The role of temporal cortex in the control of attention. *Curr. Res. Neurobiol.* **3**, 100038 (2022).
53. Peck, C. J., Lau, B. & Salzman, C. D. The primate amygdala combines information about space and value. *Nat. Neurosci.* **16**, 340–348 (2013).
54. Knight, R. T. Contribution of human hippocampal region to novelty detection. *Nature* **383**, 256–259 (1996).
55. Rao, H., Zhou, T., Zhuo, Y., Fan, S. & Chen, L. Spatiotemporal activation of the two visual pathways in form discrimination and spatial location: a brain mapping study. *Hum. Brain Mapp.* **18**, 79–89 (2003).
56. Posner, M. I. Orienting of attention. *Q. J. Exp. Psychol.* **32**, 3–25 (1980).
57. Corbetta, M. & Shulman, G. L. Control of goal-directed and stimulus-driven attention in the brain. *Nat. Rev. Neurosci.* **3**, 201–215 (2002).
58. Vossel, S., Geng, J. J. & Fink, G. R. Dorsal and ventral attention systems: distinct neural circuits but collaborative roles. *Neuroscientist* **20**, 150–159 (2014).
59. Van Rossum, G. & Drake, F. L. Python Reference Manual <http://docs.python.org> (2006).
60. Delorme, A. & Makeig, S. EEGLAB: an open source toolbox for analysis of single-trial EEG dynamics including independent component analysis. *J. Neurosci. Methods* **134**, 9–21 (2004).
61. Lopez-Calderon, J. & Luck, S. J. ERPLAB: an open-source toolbox for the analysis of event-related potentials. *Front. Hum. Neurosci.* **8**, 213 (2014).
62. Liu, J. et al. Stable maintenance of multiple representational formats in human visual short-term memory. *Proc. Natl Acad. Sci. USA* **117**, 32329–32339 (2020).
63. Bijanzadeh, M. et al. Decoding naturalistic affective behaviour from spectro-spatial features in multiday human iEEG. *Nat. Hum. Behav.* **6**, 823–836 (2022).
64. Grossman, S. et al. Convergent evolution of face spaces across human face-selective neuronal groups and deep convolutional networks. *Nat. Commun.* **10**, 4934 (2019).

65. Feldmann-Wüstefeld, T., Weinberger, M. & Awh, E. Spatially guided distractor suppression during visual search. *J. Neurosci.* **41**, 3180–3191 (2021).
66. Gaspelin, N., Leonard, C. J. & Luck, S. J. Suppression of overt attentional capture by salient-but-irrelevant color singletons. *Atten. Percept. Psychophys.* **79**, 45–62 (2017).
67. Wang, B., Samara, I. & Theeuwes, J. Statistical regularities bias overt attention. *Atten. Percept. Psychophys.* **81**, 1813–1821 (2019).
68. Fischl, B., Sereno, M. I. & Dale, A. M. Cortical surface-based analysis: II: inflation, flattening, and a surface-based coordinate system. *NeuroImage* **9**, 195–207 (1999).
69. Groppe, D. M. et al. iELVis: an open source MATLAB toolbox for localizing and visualizing human intracranial electrode data. *J. Neurosci. Methods* **281**, 40–48 (2017).
70. Mukamel, R. et al. Coupling between neuronal firing, field potentials, and fMRI in human auditory cortex. *Science* **309**, 951–954 (2005).
71. Parvizi, J. & Kastner, S. Promises and limitations of human intracranial electroencephalography. *Nat. Neurosci.* **21**, 474–483 (2018).
72. Watson, B. O., Ding, M. & Buzsáki, G. Temporal coupling of field potentials and action potentials in the neocortex. *Eur. J. Neurosci.* **48**, 2482–2497 (2018).
73. Jensen, O., Kaiser, J. & Lachaux, J.-P. Human gamma-frequency oscillations associated with attention and memory. *Trends Neurosci.* **30**, 317–324 (2007).
74. Benjamini, Y. & Yekutieli, D. The control of the false discovery rate in multiple testing under dependency. *Ann. Stat.* **29**, 1165–1188 (2001).
75. Norman, Y., Yeagle, E. M., Harel, M., Mehta, A. D. & Malach, R. Neuronal baseline shifts underlying boundary setting during free recall. *Nat. Commun.* **8**, 1301 (2017).
76. Miller, J., Patterson, T. & Ulrich, R. Jackknife-based method for measuring LRP onset latency differences. *Psychophysiology* **35**, 99–115 (1998).
77. Wang, L., Kuperberg, G. & Jensen, O. Specific lexico-semantic predictions are associated with unique spatial and temporal patterns of neural activity. *eLife* **7**, e39061 (2018).
78. Wang, B. Shared_data, *GitHub*, https://github.com/wangbenchi/Shared_data (2024).

Acknowledgements

This research was supported by the National Science and Technology Innovation 2030 Major Program (grant no. 2022ZD0204802 to B.W.), the National Natural Science Foundation of China (grant no. 32000738 to B.W.) and the Sanming Project of Medicine in Shenzhen (grant no. SZSM202003006 to X.M.). The funders had no role in study design, data collection and analysis, decision to publish or preparation of the manuscript.

Author contributions

R.L., X.M., F.C., X.L. and B.W. designed the experiment. R.L., X.M. and F.C. collected the data. R.L. and B.W. analysed the data. R.L., O.J., J.T. and B.W. wrote the paper.

Competing interests

The authors declare no competing interests.

Additional information

Supplementary information The online version contains supplementary material available at <https://doi.org/10.1038/s41562-024-01852-5>.

Correspondence and requests for materials should be addressed to Benchi Wang.

Peer review information *Nature Human Behaviour* thanks Jacqueline Gottlieb and the other, anonymous, reviewer(s) for their contribution to the peer review of this work. Peer reviewer reports are available.

Reprints and permissions information is available at www.nature.com/reprints.

Publisher's note Springer Nature remains neutral with regard to jurisdictional claims in published maps and institutional affiliations.

Springer Nature or its licensor (e.g. a society or other partner) holds exclusive rights to this article under a publishing agreement with the author(s) or other rightsholder(s); author self-archiving of the accepted manuscript version of this article is solely governed by the terms of such publishing agreement and applicable law.

© The Author(s), under exclusive licence to Springer Nature Limited 2024

Reporting Summary

Nature Portfolio wishes to improve the reproducibility of the work that we publish. This form provides structure for consistency and transparency in reporting. For further information on Nature Portfolio policies, see our [Editorial Policies](#) and the [Editorial Policy Checklist](#).

Statistics

For all statistical analyses, confirm that the following items are present in the figure legend, table legend, main text, or Methods section.

n/a Confirmed

- The exact sample size (n) for each experimental group/condition, given as a discrete number and unit of measurement
- A statement on whether measurements were taken from distinct samples or whether the same sample was measured repeatedly
- The statistical test(s) used AND whether they are one- or two-sided
Only common tests should be described solely by name; describe more complex techniques in the Methods section.
- A description of all covariates tested
- A description of any assumptions or corrections, such as tests of normality and adjustment for multiple comparisons
- A full description of the statistical parameters including central tendency (e.g. means) or other basic estimates (e.g. regression coefficient) AND variation (e.g. standard deviation) or associated estimates of uncertainty (e.g. confidence intervals)
- For null hypothesis testing, the test statistic (e.g. F , t , r) with confidence intervals, effect sizes, degrees of freedom and P value noted
Give P values as exact values whenever suitable.
- For Bayesian analysis, information on the choice of priors and Markov chain Monte Carlo settings
- For hierarchical and complex designs, identification of the appropriate level for tests and full reporting of outcomes
- Estimates of effect sizes (e.g. Cohen's d , Pearson's r), indicating how they were calculated

Our web collection on [statistics for biologists](#) contains articles on many of the points above.

Software and code

Policy information about [availability of computer code](#)

Data collection

Data analysis

All manuscripts utilizing custom algorithms or software that are central to the research but not yet described in published literature, software must be made available to editors and reviewers. We strongly encourage code deposition in a community repository (e.g. GitHub). See the Nature Portfolio [guidelines for submitting code & software](#) for further information.

Data

Policy information about [availability of data](#)

All manuscripts must include a [data availability statement](#). This statement should provide the following information, where applicable:

- Accession codes, unique identifiers, or web links for publicly available datasets
- A description of any restrictions on data availability
- For clinical datasets or third party data, please ensure that the statement adheres to our [policy](#)

Research involving human participants, their data, or biological material

Policy information about studies with [human participants or human data](#). See also policy information about [sex, gender \(identity/presentation\), and sexual orientation](#) and [race, ethnicity and racism](#).

Reporting on sex and gender	Sex and gender were not considered in the present study, as we assumed that they all have the same cognitive processing.
Reporting on race, ethnicity, or other socially relevant groupings	Not applicable.
Population characteristics	We have eighteen patients (9 males and 9 females, ages 21– 58) .
Recruitment	Participants were randomly selected based on their wish. There was no self-selection bias. . All participants gave verbal or written informed consent to participate in research, with no monetary compensation.
Ethics oversight	the Medical Ethics Committee of Shenzhen University General Hospital (2018012)

Note that full information on the approval of the study protocol must also be provided in the manuscript.

Field-specific reporting

Please select the one below that is the best fit for your research. If you are not sure, read the appropriate sections before making your selection.

Life sciences Behavioural & social sciences Ecological, evolutionary & environmental sciences

For a reference copy of the document with all sections, see [nature.com/documents/nr-reporting-summary-flat.pdf](https://www.nature.com/documents/nr-reporting-summary-flat.pdf)

Life sciences study design

All studies must disclose on these points even when the disclosure is negative.

Sample size	Sample size was predetermined according to the studies regarding attentional capture over last 30 years (e.g., Theeuwes, 1992). Normally, with a group of 18 participants, one will observe a very stable attentional capture effect, which was investigated in the present study.
Data exclusions	No data exclusion
Replication	We indeed used multiple methods with slightly changed parameters to re-analyze the data, all results were consistent. And with the new method used in the present study, we examined this with 3 different datasets, all of them worked.
Randomization	All participants needed finish all the testing conditions, it is a within-subjects design.
Blinding	We did not have group allocation.

Reporting for specific materials, systems and methods

We require information from authors about some types of materials, experimental systems and methods used in many studies. Here, indicate whether each material, system or method listed is relevant to your study. If you are not sure if a list item applies to your research, read the appropriate section before selecting a response.

Materials & experimental systems

n/a	Involvement in the study
<input checked="" type="checkbox"/>	<input type="checkbox"/> Antibodies
<input checked="" type="checkbox"/>	<input type="checkbox"/> Eukaryotic cell lines
<input checked="" type="checkbox"/>	<input type="checkbox"/> Palaeontology and archaeology
<input checked="" type="checkbox"/>	<input type="checkbox"/> Animals and other organisms
<input checked="" type="checkbox"/>	<input type="checkbox"/> Clinical data
<input checked="" type="checkbox"/>	<input type="checkbox"/> Dual use research of concern
<input checked="" type="checkbox"/>	<input type="checkbox"/> Plants

Methods

n/a	Involvement in the study
<input checked="" type="checkbox"/>	<input type="checkbox"/> ChIP-seq
<input checked="" type="checkbox"/>	<input type="checkbox"/> Flow cytometry
<input type="checkbox"/>	<input checked="" type="checkbox"/> MRI-based neuroimaging

Magnetic resonance imaging

Experimental design

Design type	Acquired T1-weighted MR images
Design specifications	We only used MRI-based neuroimaging method to obtain T1-weighted MR images for getting the locations of electrodes in iEEG recordings.
Behavioral performance measures	No task was used during MRI scan.

Acquisition

Imaging type(s)	structural
Field strength	3T
Sequence & imaging parameters	T1-weighted MR images, Sequence=GR\IR, TR=2200ms, TE=2.98ms, Matrix=[0,256,256,0], Flip angle=9, Slice thickness=0.5.
Area of acquisition	whole brain scan
Diffusion MRI	<input type="checkbox"/> Used <input type="checkbox"/> Not used

Preprocessing

Preprocessing software	FreeSurfer v6.0.0 for segmentation and registration.
Normalization	Liner normalization
Normalization template	MNI space
Noise and artifact removal	Not applicable
Volume censoring	Not applicable

Statistical modeling & inference

Model type and settings	Not applicable
Effect(s) tested	Not applicable
Specify type of analysis:	<input checked="" type="checkbox"/> Whole brain <input type="checkbox"/> ROI-based <input type="checkbox"/> Both
Statistic type for inference	Not applicable
(See Eklund et al. 2016)	
Correction	Not applicable

Models & analysis

n/a	Involvement in the study
<input checked="" type="checkbox"/>	<input type="checkbox"/> Functional and/or effective connectivity
<input checked="" type="checkbox"/>	<input type="checkbox"/> Graph analysis
<input checked="" type="checkbox"/>	<input type="checkbox"/> Multivariate modeling or predictive analysis